Published OnlineFirst March 16, 2015; DOI: 10.1158/1535-7163.MCT-14-1092

Molecular Cancer Therapeutics

Synthetic Lethal Screens Identify Vulnerabilities in GPCR Signaling and Cytoskeletal Organization in E-Cadherin–Deficient Cells

Bryony J. Telford[1], Augustine Chen[1], Henry Beetham[1], James Frick[1], Tom P. Brew[1], Cathryn M. Gould[2], Andrew Single[1], Tanis Godwin[1], Kaylene J. Simpson[2,3], and Parry Guilford[1]

Abstract

The *CDH1* gene, which encodes the cell-to-cell adhesion protein E-cadherin, is frequently mutated in lobular breast cancer (LBC) and diffuse gastric cancer (DGC). However, because E-cadherin is a tumor suppressor protein and lost from the cancer cell, it is not a conventional drug target. To overcome this, we have taken a synthetic lethal approach to determine whether the loss of E-cadherin creates druggable vulnerabilities. We first conducted a genome-wide siRNA screen of isogenic MCF10A cells with and without *CDH1* expression. Gene ontology analysis demonstrated that G-protein–coupled receptor (GPCR) signaling proteins were highly enriched among the synthetic lethal candidates. Diverse families of cytoskeletal proteins were also frequently represented. These broad classes of E-cadherin synthetic lethal hits were validated using both lentiviral-mediated shRNA knockdown and specific antagonists, including the JAK inhibitor LY2784544, Pertussis toxin, and the aurora kinase inhibitors alisertib and danusertib. Next, we conducted a 4,057 known drug screen and time course studies on the *CDH1* isogenic MCF10A cell lines and identified additional drug classes with linkages to GPCR signaling and cytoskeletal function that showed evidence of E-cadherin synthetic lethality. These included multiple histone deacetylase inhibitors, including vorinostat and entinostat, PI3K inhibitors, and the tyrosine kinase inhibitors crizotinib and saracatinib. Together, these results demonstrate that E-cadherin loss creates druggable vulnerabilities that have the potential to improve the management of both sporadic and familial LBC and DGC. *Mol Cancer Ther; 14(5); 1213–23. ©2015 AACR.*

Introduction

E-cadherin is a cell-to-cell adhesion protein that is localized at the adherens junction of all epithelial cells (1). Other than its roles in cell adhesion, E-cadherin is involved in establishing and maintaining cell polarity and differentiation, the organization of cell migration and architecture and the mediation of signaling through various proliferation and survival pathways, including WNT and EGFR (2, 3).

Abrogation of expression of the E-cadherin gene (*CDH1*) by mutation, deletion, or promoter hypermethylation is a feature common to many epithelial tumors and its downregulation is the hallmark of both diffuse gastric cancer (DGC) and lobular breast cancer (LBC; refs. 1, 4–6). Disrupting E-cadherin's expression or localization has a pronounced impact on a cell's cytoskeletal structure, with changes including misalignment of the microtubule and actin cytoskeletons, defects in cell migration and irregularities in the orientation of the mitotic spindle (7–9).

Germline *CDH1* mutations are responsible for hereditary diffuse gastric cancer (HDGC), a cancer syndrome characterized by the highly penetrant, early onset of multifocal DGC and an elevated rate of LBC. In HDGC, *CDH1* inactivation is an initiating event that may be related to abnormal mitotic spindle orientation resulting in daughter cells being displaced into the lamina propria, outside the epithelial plane (10–12). In other cancer types, its downregulation is considered to be a late event that promotes increased invasive capacity, frequently through association with the epithelial–mesenchymal transition (13).

Although E-cadherin is a tumor suppressor protein that is lost from the cancer cell and therefore not a conventional drug target, the downregulation of such a multifunctional protein during tumorigenesis would be predicted to create vulnerabilities in the cell which are targetable using a synthetic lethal approach. In the context of drug development, synthetic lethality can be defined as a drug that reduces cell viability or fitness only in cells carrying a specific mutation. The utility of synthetic lethal targeting of tumor suppressor genes is well illustrated clinically by olaparib, an inhibitor of the DNA repair enzyme PARP. Olaparib elicits strong clinical responses in breast and ovarian cancer patients who harbor inactivating mutations in the homologous recombination dsDNA repair genes *BRCA1/2* (14, 15).

[1]Cancer Genetics Laboratory, Department of Biochemistry, University of Otago, Dunedin, New Zealand. [2]Victorian Centre for Functional Genomics, Peter MacCallum Cancer Centre, East Melbourne, Victoria, Australia. [3]The Sir Peter MacCallum Department of Oncology, The University of Melbourne, Parkville, Victoria, Australia.

Note: Supplementary data for this article are available at Molecular Cancer Therapeutics Online (http://mct.aacrjournals.org/).

Current address for C.M. Gould: Garvan Institute of Medical Research, Darlinghurst, New South Wales 2010, Australia.

Corresponding Author: Parry Guilford, Cancer Genetics Laboratory, Centre for Translational Cancer Research, Department of Biochemistry, University of Otago, P.O. Box 56, Dunedin 9054, New Zealand. Phone: 643-479-7673; Fax: 643-479-5077; E-mail: parry.guilford@otago.ac.nz

doi: 10.1158/1535-7163.MCT-14-1092

Published OnlineFirst March 16, 2015; DOI: 10.1158/1535-7163.MCT-14-1092

In addition to providing new therapeutic avenues for the treatment of sporadic epithelial cancers, synthetic lethal targeting of E-cadherin–deficient cells also has the potential to improve the clinical management of HDGC. To identify druggable synthetic lethal vulnerabilities in E-cadherin–deficient cells, we have conducted both a genome-wide siRNA synthetic lethal screen and a four thousand compound known drug screen on isogenic breast MCF10A cells with and without *CDH1* expression. Together, these screens have identified multiple druggable targets that suggest new therapeutic strategies for the treatment of E-cadherin–deficient cancers and the chemoprevention of HDGC.

Materials and Methods

Cell lines and media

The MCF10A breast cell line and its paired isogenic MCF10A *CDH1*$^{-/-}$ line (here designated *CDH1*$^{-/-}$) were obtained from Sigma Aldrich in 2011 (parental line ATCC CRL-10317) and had been authenticated using short terminal repeat analysis. *CDH1*$^{-/-}$ had been created by homozygous deletion of 4 bp from exon 11 of the *CDH1* gene. The lines were resuscitated within one week of receipt and early passage cells (passage 3–7) were aliquoted and frozen. All experiments were conducted with cells between passages 6–15 in DMEM F12 media with glutamate, 5% horse serum, 20 ng/mL EGF, 0.5 μg/mL hydrocortisone, 100 ng/mL cholera toxin, and 10 μg/mL insulin. Characterization of the cell line pair is described elsewhere (7).

siRNA high-throughput screen

Cells were transfected with siRNAs from the Dharmacon SMARTpool whole genome protein-coding siRNA library (RefSeq 27) housed in the Victorian Center for Functional Genomics. Each SMARTpool contained four siRNAs that targeted different regions of each gene in one well. Each reaction, in a white walled, clear-bottom 384-well plate format, contained 0.125% DharmaFECT 3 (0.05 μL), 27.4% OptiMEM (Invitrogen), and 40 nmol/L of the siRNA SMARTpool (total volume 37.5 μL). Cells were reverse transfected and seeded onto the siRNA cocktail at a density of 700 MCF10A cells per well and 900 *CDH1*$^{-/-}$ cells/well to enable the two cell lines to reach confluence at the same time point (72 hours after seeding). The following controls were included in each plate: the death controls si*EGFR* and si*PLK1* (4 wells each), a synthetic lethal control si*CTNNB1* (6 wells) and two negative controls, siRISC free and mock (lipid only, 9 wells each). After 24 hours, the media was replaced and at 72 hours 10 μL CellTiter-Glo was added to each well (final concentration 1/5), shaken on an orbital shaker for 2 minutes and incubated for a further 30 minutes at room temperature before measuring luminescence using a Synergy H4 microplate reader (Biotek). siRNA was dispensed using a Caliper Sciclone ALH3000 (PerkinElmer). All other liquid handling steps were performed using a Biotek406 liquid handling workstation. Primary screen analysis was performed by normalizing genes in each cell line individually to the average mock value (across all screen plates) for the respective cell line. The level of increased kill was determined by the ratio of *CDH1*$^{-/-}$ viability to MCF10A viability. Candidates with MCF10A viability $\geq$50% and a fold change ratio of $\leq$0.85 were considered synthetic lethal candidates. Selection of the final 500 genes chosen for secondary screening was based on further analysis of druggability and biologic relevance. Secondary siRNA screening was performed using four individual siRNAs targeting each gene arrayed in individual wells, separately using the same transfection conditions described above with a final siRNA concentration of 25 nmol/L. The secondary screen was analyzed using the same normalization strategy and cutoffs as the primary screen.

Viral knockdown

Dharmacon pGIPZ lentiviral shRNA mir30 plasmids were prepared from cultures using the Machery Nagel EasyPure Miniprep Kit. 293FT cells were cotransfected 24 hours after seeding with 18.6 μg pGIPZ, 9.6 μg PAX2, and 4.8 μg VSVG plasmids using 55.7 μL Lipofectamine 2000 (Invitrogen). Media was changed at 24 hours, and after a further 24 hours, viral particles were harvested by aspirating media, centrifugation at 3,000 rpm for 15 minutes to remove cellular debris and filtration through a 0.45 μmol/L polyvinylidene difluoride filter. Virus was aliquoted and snap frozen for subsequent use.

Viral titer was determined by seeding MCF10A cells at 4,000 cells per well and transducing with a 1/32 dilution of virus 24 hours later. Media was changed after 24 hours, and after a further 24 hours, GFP-expressing cells were quantitated over 5 fields at 10× magnification. The average number of transduced cells per well was used to determine the number of transducing units per mL.

For knockdown experiments, 1,000 MCF10A and 2,000 *CDH1*$^{-/-}$ cells per well were seeded in black walled, clear bottomed 96-well plates and allowed to adhere overnight. The following day, virus was added at a multiplicity of infection (MOI) of 10. Media were changed at 24 hours and 1 μg/mL puromycin added. Seventy-four hours after transduction, media was aspirated and 1 μg/mL Hoechst 33342 and 0.5 μg/mL propidium iodide in PBS added. After 30 minutes, incubation plates were imaged with 4 fields per well on the Cytell (GE) at 4× magnification and 10 fields per well at 10× magnification using the "Cell Viability BioApp". CellProfiler (16) was used to quantitate the total nuclei, as well as the proportion stained with propidium iodide.

RNA was extracted at 72 hours to determine gene knockdown using the RNAgem-PLUS Kit (ZyGem). cDNA was synthesized using the Primescript cDNA Synthesis Kit (Takara), and qPCR performed using Sybr Fast kit (KAPA) on an ABI7900HT with an enzyme activation step of 95°C for 3 minutes followed by 40 cycles of 95°C for 15 seconds, 57°C for 15 seconds, and 72°C for 15 seconds. *GAPDH* and *PPIA* were used as reference genes and results were analyzed using the efficiency method as described by Pfaffl (17).

Known drug screen

Assay ready plates containing 20 nL of 4,057 compounds diluted in DMSO at four concentrations (2, 1, 0.5, and 0.25 μmol/L) were prepared by the Walter and Eliza Hall Institute (WEHI, Parkville, Victoria, Australia) High-Throughput Chemical Screening Facility. Cells were seeded directly onto these plates in a volume of 50 μL at a density of 1,000 cells per well for MCF10A and 1,200 cells per well for *CDH1*$^{-/-}$ in 384-well clear bottom plates. After 48 hours, 20 μL of CellTiter-Glo (Promega) was added to each well, shaken for 2 minutes on an orbital shaker, and incubated for 30 minutes before reading. Values were normalised to the average DMSO control value of the whole screen for each cell line at each concentration.

The secondary drug screen was performed on 316 compounds selected from the primary screen. These were provided at 5 mmol/L

Published OnlineFirst March 16, 2015; DOI: 10.1158/1535-7163.MCT-14-1092

and 11 1:1 dilutions were made with DMSO to create a 10 μmol/L to 10 nmol/L concentration range. Cells were seeded at a density of 700 cells per well for MCF10A and 900 cells per well for *CDH1*$^{-/-}$ for 24 hours before 100 nL of each compound was added to the plates robotically. Thirty-two DMSO control wells were included in each plate. Plates were incubated for a further 48 hours before assaying with CellTiter-Glo.

Drug titrations and time course assays

To determine drug EC_{50}, cells were seeded in white walled, clear-bottom 384 well plates at a density of 800 cells per well in a volume of 45 μL. After 24 hours incubation, 5 μL of drug (rehydrated in DMSO to an 80 mmol/L stock and diluted in complete media) was added to each well. A DMSO control and a cell only control were used on each plate. The 11 drug concentrations used were dependent on the individual drug. After 48 hours of treatment, cell viability was assayed using either the CellTiter-Glo (Promega) or Alamar blue assay. All results were normalized to the average DMSO control for individual cell types. EC_{50} values were calculated by plotting viability against the log drug concentration and fitting a nonlinear regression curve using Prism version 6.0 for Mac (GraphPad Software).

Drug time course assays were carried out by seeding equal numbers of MCF10A or *CDH1*$^{-/-}$ at 4,000 cells per well in xCELLigence plates (Roche), except for crizotinib which was seeded at 2,000 cells per well. The xCELLigence system measures relative changes in electrical impedance in a well ("cell proliferation index") which can be used as a measure of cell number. After 24 hours, three concentrations of each drug were added and growth followed in real time for a further 72 hours. Assays were carried out in duplicate and the data averaged. Time course assays were also performed on the IncuCyte Imaging System (Essen Bioscience). Cells were seeded at 4,000 cells per well in black walled clear-bottom 96-well plates. After 24 hours, five concentrations of each drug were added and 3 fields were imaged per well at 4× magnification every 2 hours for 48 hours. Plates were then removed and cell numbers determined using metabolic assays and nuclei imaging as described above.

For drug synergy studies, the combination index was determined using CompuSyn software (ComboSyn Inc) and the Chou–Talalay method (18). EC_{50} was estimated for both drugs and cells treated with each drug alone and in combination at this concentration and concentrations 2- and 4-fold higher and lower. Viability was calculated by nuclei counting and normalized values imported into CompuSyn.

Results

Genome-wide siRNA screen of *CDH1* isogenic MCF10A cells

To identify genes potentially involved in a synthetic lethal interaction with E-cadherin, we conducted a genome-wide functional screen using the Dharmacon siGENOME SMARTpool library targeting 18,120 genes in a pooled format, with 4 individual siRNAs targeting each gene. Isogenic MCF10A cells with and without *CDH1* expression were screened in parallel, and viability was assayed 72 hours after transduction using CellTiter-Glo. si*PLK1* and si*EGFR* were used as positive death controls (Fig. 1A) and si*CTNNB1* used as a positive synthetic lethal control, after showing a mild synthetic lethal effect in a pilot screen (Supplementary Fig. S1). Mock (lipid only) and RISC-free control (Dharmacon) were included as nontargeting controls. Little variability was observed between these controls; consequently, we normalized the values of each gene to the average screen-wide mock value within each cell line. Hits were selected on the basis of

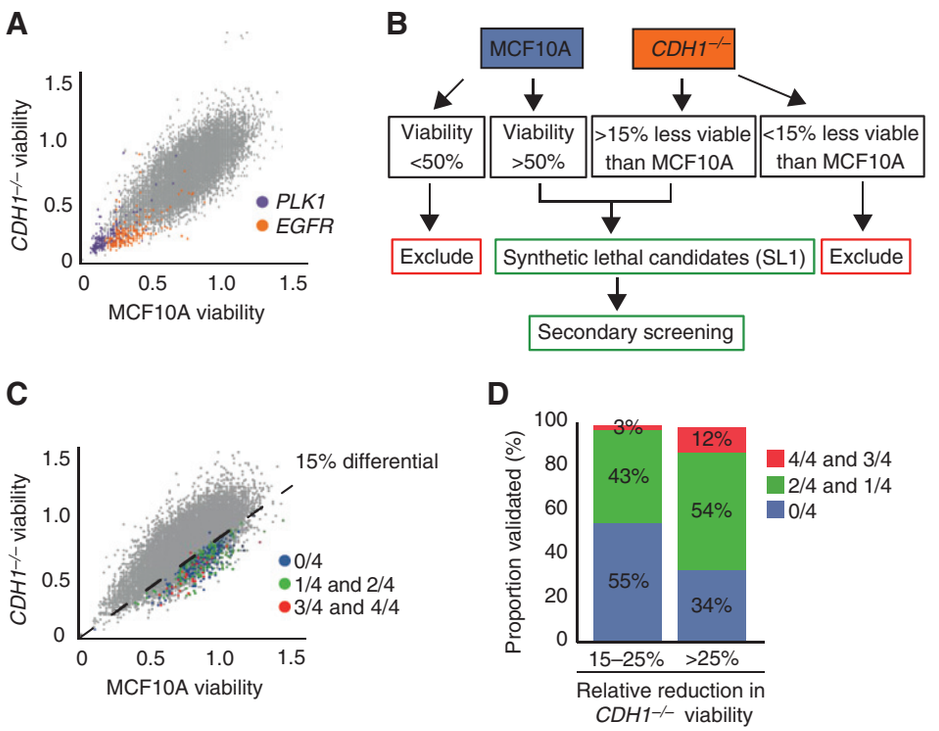

Figure 1.
siRNA screening overview of outcomes and analysis strategy. A, the resulting effect on cell viability after knockdown of each protein-coding target in MCF10A and *CDH1*$^{-/-}$ cells. The positive death controls si*PLK1* and si*EGFR* both consistently cause death in both cell lines. B, the analysis workflow used to select synthetic lethal candidates based on MCF10A and *CDH1*$^{-/-}$ viability. C, correlation between primary and secondary screens. The dotted line marks where *CDH1*$^{-/-}$ has 15% less viability than MCF10A. The primary screen identified 500 candidates that were selected for validation in a secondary screen. Five percent of these validates as with 3 of 4 or 4 of 4 individual siRNA. D, candidates tested in the secondary screen were split into two categories, based on the decrease in viability of *CDH1*$^{-/-}$ compared with MCF10A. Candidates with a greater differential were more likely to be validated in the secondary screen.

Published OnlineFirst March 16, 2015; DOI: 10.1158/1535-7163.MCT-14-1092

the ratio of cell viability between the MCF10A and *CDH1*$^{-/-}$ cells 72 hours after transduction (Fig. 1B). We rejected siRNAs that were highly toxic to the MCF10A cells (a decrease in viability of ≥50%) and selected those for which the viability of *CDH1*$^{-/-}$ cells decreased by ≥15% more than the corresponding knockdown in MCF10A cells. These targets were classed as *CDH1* synthetic lethal candidate genes (List SL1, 2,437 genes; Supplementary Table S1). From this set, 501 genes were manually selected for secondary screening using criteria, including predicted druggability of the encoded proteins and biologic significance. The secondary screen was performed by deconvoluting the four individual siRNAs that consititute the SMARTpool. Using the same stringent threshold as the primary screen (i.e., MCF10A viability ≥50% and ≥15% more death in *CDH1*$^{-/-}$), 21 genes (5%) had 3 of 4 or 4 of 4 of the individual siRNAs show a synthetic lethal effect. One hundred eighty-three genes (44%) had 1 of 4 or 2 of 4 siRNAs validated. Fifty-one percent of genes were not validated (0/4) by this approach. Division of the selected genes into groups based on the strength of the synthetic lethal phenotype in the primary screen demonstrated that candidates which showed a greater viability differential between MCF10A and *CDH1*$^{-/-}$ cells were more likely to be validated in the secondary screen (Fig. 1C and D). Of the candidates that reduced *CDH1*$^{-/-}$ cell number by ≥25% more than MCF10A cells, 12% validated with 3 of 4 or 4 of 4 individual siRNAs, a validation rate comparable with other genome-wide RNAi studies (19, 20).

Functional diversity: gene ontology analysis

To search for functional enrichment in the 2,437 synthetic lethal candidates identified in the primary screen (List SL1), we conducted a gene ontology analysis using DAVID (21). Using the Functional Annotation Clustering tool, the most enriched functional cluster was a group of ten terms associated with G-protein–coupled receptor (GPCR) signaling (enrichment score = 10.01; Supplementary Table S2A). Accordingly, the two most significant biologic process terms (Supplementary Table S2B) were "G-protein–coupled receptor protein signaling pathway" (Benjamini-adjusted *P* value = 4.1×10^{-8}) and "cell surface receptor linked signal transduction" (adj. *P* value = 1.7×10^{-5}). These cell signaling processes were strongly reflected in the DAVID gene ontology molecular function terms (Supplementary Table S2C) which included peptide, neuropeptide, and purinergic nucleotide receptor activity and protein kinase activity (adj. *P* value 3.5×10^{-7} to 3.2×10^{-2}).

Because our ultimate goal is to identify targeted drugs for E-cadherin–deficient tumors that have minimal toxicity against nonmalignant tissues, we also performed gene ontology analysis on a subset of genes from List SL1 whose corresponding siRNA SMARTpools had little or no impact on MCF10A cells (MCF10A viability ≥0.85 mock). 1,136 genes met this revised threshold (List SL2; Supplementary Table S3). Notably, this more stringent cutoff led to further enrichment of both the GPCR-associated functional cluster (enrichment score, 12.14) and the biologic process terms "GPCR protein signaling pathway" (adj. *P* value = $9.0 \times 10^{-}16$) and "cell surface receptor linked signal transduction" (adj. *P* value = 4.8×10^{-10}; Supplementary Table S2D).

Our earlier observation of abnormal cytoskeletal organization in E-cadherin–deficient MCF10A cells (7) prompted us to look for specific cytoskeletal functions associated with synthetic lethality. Although the adjusted *P* values for cytoskeletal-like terms in List SL1 and SL2 did not reach significance, DAVID functional clusters associated with each of cell motility, cell polarity, and cell adhesion were among the top five clusters observed in the group of synthetic lethal candidate genes which reduced MCF10A viability to <0.85 of the mock controls (enrichment scores, 2.18, 1.97, and 1.84, respectively; Supplementary Table S2E). This greater representation of cytoskeletal genes among synthetic lethal candidates that seriously affect MCF10A cell viability presumably reflects the essential role of many cytoskeletal proteins. Cyto- or nucleoskeletal functions that were represented in List SL1, often by multiple family members, included microtubule nucleation, organization, and function (e.g., *TUBA1C*, *TUBG1*, *TUBB2A*, *MZT2A*, *ARPC3*, *NME4*, *NME7*, *MAST1*, *MAST2*, *MAST3*, *NEK1*, *NEK3*, *NEK4*, *NEK10*, *CLIP1*, *CLIP2*, *TEKT3*, *TEKT4*, *TEKT5*), Rho-mediated motility (e.g., *RHOB*, *RHOC*, *RHOH*, *RAC1*, *PAK2*, *TIAM1*), linkages between the cytoskeleton and nucleoskeleton (e.g., *SUN1*, *SUN2*, *SUN5*, *NSUN3*, *NSUN6*, *SYNE1*), polarity (e.g., *DLG1*, *DLG2*, *DLG4*, *DLG5*, *CELSR1*, *CELSR3*), and actin filament organization and remodeling (e.g., *AVIL*, *ARF6*, *CYTH2*, *CTYH3*, *CYTH4*).

E-cadherin–deficient MCF10A cells are sensitive to downregulation of microtubule-associated genes and the aurora kinase A inhibitor alisertib

To validate the apparent synthetic lethal interaction between E-cadherin and the microtubule cytoskeleton, we selected three microtubule-associated genes, *MAST2*, *MAP1B*, and *MAPRE3* for confirmation using lentiviral shRNA knockdown. MAST2 is a microtubule-associated serine–threonine kinase (22); MAP1B is a microtubule-binding and -stabilizing protein that can also interact with actin microfilaments (23) and MAPRE3 is a microtubule plus end-binding protein involved in regulating the dynamics of microtubules and their interactions with intracellular structures such as the cell cortex or mitotic kinetochore (24). These three genes had previously been validated in the secondary screen, with 3 of 4, 2 of 4, and 1 of 4 siRNAs, respectively, decreasing the viability of *CDH1*$^{-/-}$ cells by at least 15% more than the MCF10A (Fig. 2A). shRNAs targeting these three genes resulted in 51%–86% mRNA knockdown in both cell lines (Fig. 2B). Seventy-two hours after transduction, cell viability was measured using nuclei counting (Fig. 2C). Knockdown of each of *MAP1B*, *MAST2*, and *MAPRE3* resulted in 15%–29% more cell death in the *CDH1*$^{-/-}$ cells compared with the MCF10A cells, confirming the siRNA data.

To determine whether the synthetic lethal phenotype observed with downregulation of microtubule-associated genes could be recapitulated using known inhibitors of microtubule function, we treated the isogenic MCF10A cell line pair with the microtubule stabilizing drug taxol and inhibitors of the microtubule-associated proteins aurora kinase A and aurora kinase B. Increasing concentrations of taxol (1–16 nmol/L) led to a small increase in cell death in *CDH1*$^{-/-}$ cells compared with MCF10A cells (Supplementary Fig. S2). The aurora kinase A inhibitor alisertib and the aurora kinase B inhibitor danusertib both showed a minor synthetic lethal effect (Fig. 2D and E), with 18% (at 25 nmol/L) and 12% (50 nmol/L) more death in the *CDH1*$^{-/-}$ line, respectively. Together, the RNAi and aurora kinase inhibitor data demonstrate that E-cadherin–deficient MCF10A cells are more vulnerable to disruption of specific microtubule-related functions than E-cadherin–expressing MCF10A cells.

Published OnlineFirst March 16, 2015; DOI: 10.1158/1535-7163.MCT-14-1092

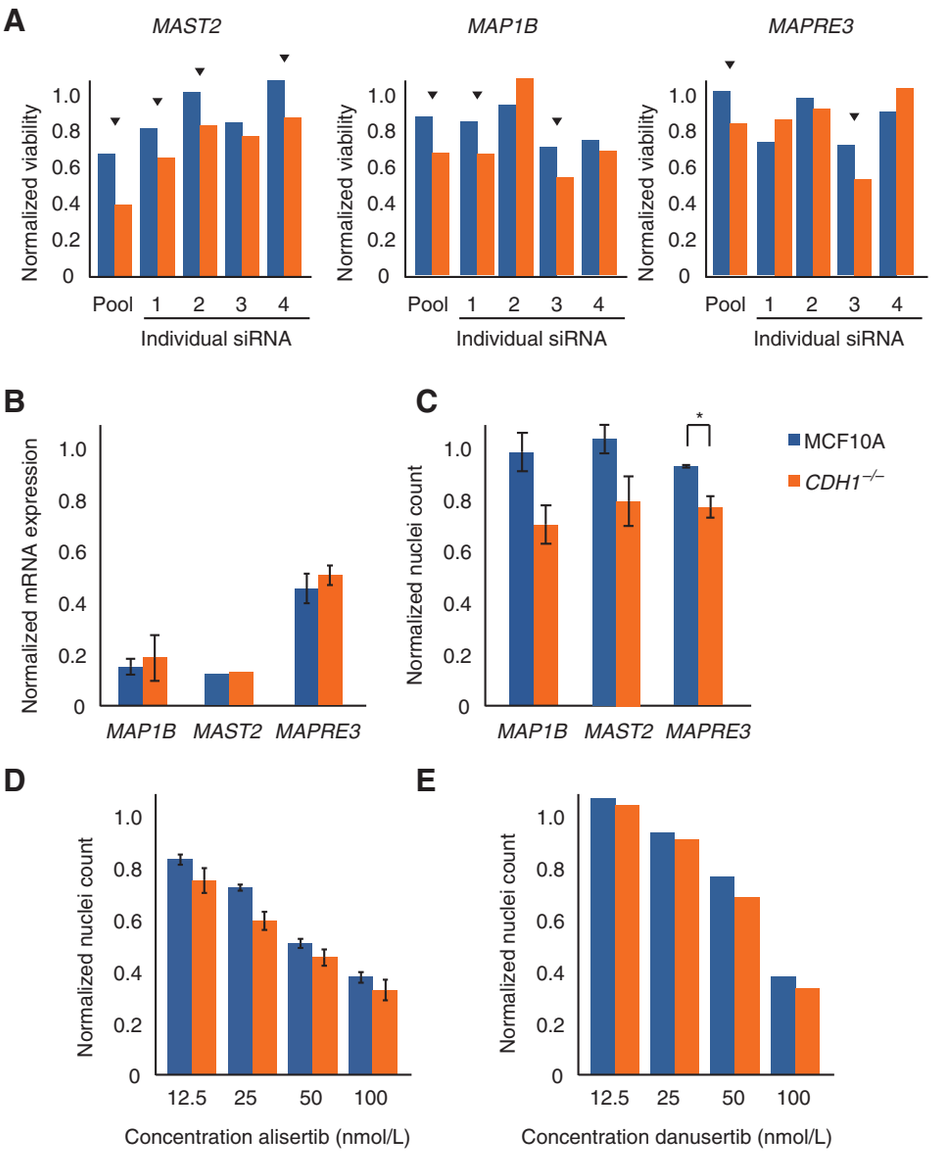

Figure 2.
Disruption of microtubule-associated proteins induces synthetic lethal effect. A, bar graphs with primary and secondary screen viability normalized to mock for *MAST2*, *MAP1B*, and *MAPRE3*. Each value is the average of two technical replicates. The arrowheads mark siRNAs that reached the synthetic lethal criteria (15% less viability in *CDH1*$^{-/-}$ cells). B, level of mRNA knockdown 72 hours after transduction with shRNA lentivirus constructs. Error bars show SE of two independent experiments, except for *MAST2* which was only assayed once. C, nuclei count normalized to nonsilencing control after knockdown with *MAP1B*, *MAST2*, and *MAPRE3* shRNA. Error bars show SE of two independent experiments. *, $P < 0.05$ by one-tailed, equal variance Student *t* test. D, nuclei count normalized to DMSO control 48 hours after alisertib treatment. Error bars show SEM of two independent experiments. E, nuclei count normalized to DMSO control 48 hours after danusertib treatment. A single experiment is shown.

E-cadherin–deficient MCF10A cells show vulnerabilities in GPCR signaling

Gene ontology analysis (21) identified >200 genes from our list of synthetic lethal candidates (List SL1) that were associated with GPCR protein signaling pathways. These candidates included several proteins involved in signal transduction from activated GPCRs such as the G protein subunits GNAS, GNAT1, GNG2, and GNG5, the membrane bound adenyl cyclase ADCY7 and the downstream signaling protein JAK2. *ADCY7* validated in the secondary screen with 4 of 4 siRNAs recapitulating the SMARTpool phenotype (Fig. 3A). The synthetic lethal effect of the *JAK2* siRNA SMARTpool was confirmed using lentiviral-mediated shRNA transduction. Both the siRNA SMARTpool and lentiviral shRNA knocked down *JAK2* mRNA by >44% (Fig. 3B). Normalized cell numbers after transduction were significantly lower in the *CDH1*$^{-/-}$ cells compared with the MCF10A cells for both the siRNA pool and the shRNA (Fig. 3C). To determine whether the synthetic lethality of *JAK2* downregulation could be mimicked using a JAK2 antagonist, we treated the isogenic *CDH1* MCF10A cell line pair with the JAK inhibitor LY2784544. Using the xCELLigence system to monitor cell growth in real time, LY2784544 had only a modest effect on MCF10A cells at 0.32, 0.63, and 1.25 μmol/L concentrations; however, the cell proliferation index was reduced in the *CDH1*$^{-/-}$ cells in a concentration-dependent manner. Forty-eight hours after drug addition, the three concentrations of LY2784544 resulted in a 15%, 29%, and 51% reduction in *CDH1*$^{-/-}$ cell number, respectively (Fig. 3D). In contrast, the three drug concentrations reduced MCF10A cell number by 0%, 11%, and 10%, respectively. A second JAK2 inhibitor, AG490, showed a similar synthetic lethal response in xCELLigence assays (data not shown). Further real-time assays using the IncuCyte replicated this effect (Supplementary Fig. S3). Nuclei counting confirmed a significant synthetic lethal effect at LY2784544 concentrations of 1.25 μmol/L

Published OnlineFirst March 16, 2015; DOI: 10.1158/1535-7163.MCT-14-1092

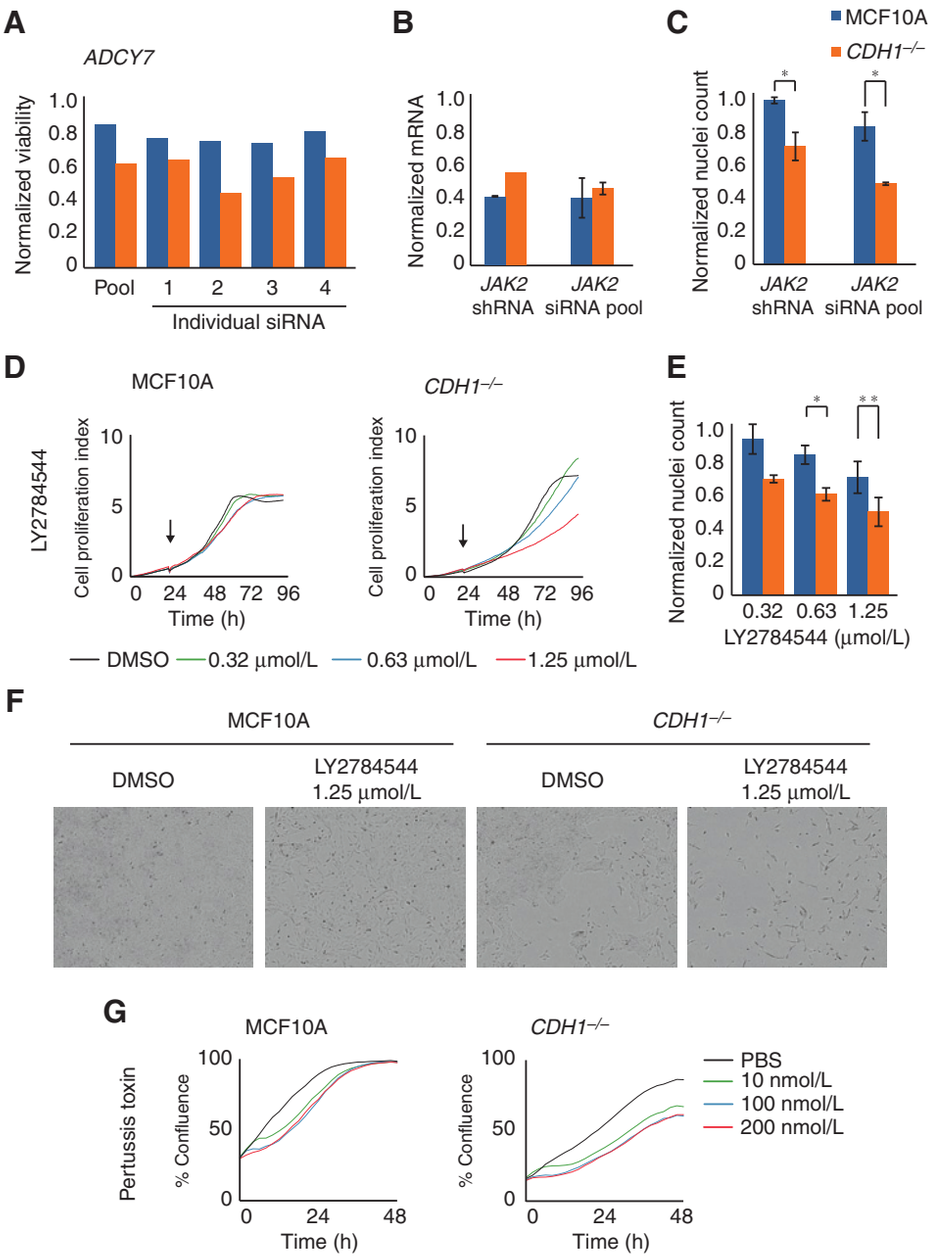

Figure 3.
Disruption of GPCR-associated proteins causes synthetic lethality. A, bar graphs with primary and secondary screen viability normalized to mock for *ADCY7*. Each value is the average of two technical replicates. All siRNA reached the synthetic lethal criteria. B, normalized mRNA levels after knockdown by *JAK2* shRNA and siRNA pool. C, nuclei counts normalized to nonsilencing (shRNA) or mock (siRNA) controls after knockdown by *JAK2* RNAi. D, representative xCELLigence experiment for cells treated with LY2784544. Arrow marks time when compound was added. E, nuclei count normalized to DMSO 48 hours after LY2784544 treatment. F, images taken 48 hours after LY2784544 treatment showing reduced confluence and morphologic changes. G, representative IncuCyte assay showing confluence over 48 hours after Pertussis toxin treatment. Error bars show SE of at least two independent experiments. *, $P < 0.05$; **, $P < 0.01$ by the one-tailed, equal variance Student *t* test.

($P = 0.005$) and 0.63 μmol/L ($P = 0.03$) (Fig. 3E). LY2784544 resulted in cells becoming more spindle shaped, with an increased number of extended filopodia; this effect was particularly marked in the *CDH1*$^{-/-}$ cells (Fig. 3F).

The presence of G protein subunits in list SL1 prompted us to examine *CDH1* synthetic lethality using the Gαi and Gαo subunit inhibitor Pertussis toxin (25). Treatment of MCF10A and *CDH1*$^{-/-}$ cells with 10, 100, and 200 ng/mL of Pertussis toxin over a period of 48 hours resulted in growth inhibition of both MCF10A and *CDH1*$^{-/-}$ cell lines in a concentration-dependent manner (Fig. 3G). However, the MCF10A cells recovered and reached the same confluence as the PBS control after 48 hours, whereas the *CDH1*$^{-/-}$ cells showed 20%–30% less confluence at that time point for the three drug concentrations.

E-cadherin loss sensitizes MCF10A cells to HDAC inhibitors and other drug classes

To explore how E-cadherin loss alters sensitivity of MCF10A cells to other known drugs, we screened 4,057 compounds against the *CDH1* MCF10A isogenic cell line pair. The compounds comprised the WEHI known drug library (3,600 compounds from the Tocriscreen Total library, the Prestwick Chemical Library and the "Lopac 1280" library), the Selleck Chemistry inhibitor library (326 compounds consisting of approximately half known drugs and half kinase inhibitors) and a kinase inhibitor library (131 compounds supplied by SYNthesis Medicinal Chemistry). The initial screen covered four drug concentrations ranging from 0.25 to 2 μmol/L, with cell viability measured at 48 hours after drug addition using the CellTiter-Glo assay. Potential synthetic

Published OnlineFirst March 16, 2015; DOI: 10.1158/1535-7163.MCT-14-1092

Table 1. Known drugs with greater inhibitory effect on *CDH1*$^{-/-}$ cells compared with MCF10A cells

Drug name	Drug class	MCF10A EC_{50} (μmol/L)	*CDH1*$^{-/-}$ EC_{50} (μmol/L)	*CDH1*$^{-/-}$ to MCF10A ratio
Mocetinostat	HDAC inhibitor	1.76	1.02	0.58
Entinostat	HDAC inhibitor	4.31	2.50	0.58
Quisinostat	HDAC inhibitor	0.05	0.04	0.72
Pracinostat	HDAC inhibitor	0.73	0.54	0.74
LAQ824	HDAC inhibitor	0.09	0.06	0.76
Panobinostat	HDAC inhibitor	0.08	0.07	0.84
Crizotinib	ROS1-like tyrosine kinase inhibitor	5.53	3.98	0.72
PI103	PI3K inhibitor	0.75	0.59	0.79
GSK2126458	PI3K inhibitor	0.05	0.04	0.79
PIK-75 hydrochloride	PI3K inhibitor	0.08	0.07	0.89
CGP 71683 hydrochloride	NPY5R inhibitor	3.92	3.47	0.89
Tyrphostin A9	PDGFR and EGFR inhibitor	1.30	0.65	0.50
AZD8055	mTOR inhibitor	0.22	0.12	0.53
Obatoclax Mesylate	BCL2 inhibitor	0.63	0.47	0.74
Brefeldin A	Guanine nucleotide exchange factor inhibitor	0.20	0.15	0.76
LY2784544	JAK family inhibitor	5.64	4.70	0.83
FCCP	uncoupler of mitochondrial oxidative phosphorylation	3.74	2.90	0.78
JNJ-7706621	CDK and aurora kinase inhibitor	3.37	2.77	0.82
Danusertib	Inhibitor of aurora kinases, Bcr-Abl, c-RET, and FGFR	1.25	1.07	0.86
PD-166285 hydrate	Broad-spectrum tyrosine kinase inhibitor	0.66	0.58	0.88
10-DEBC hydrochloride	AKT/protein kinase B inhibitor	8.10	7.26	0.90

NOTE: EC_{50} values were obtained from 11-point dilution curves carried out in duplicate. Cell viability was determined using the CellTiter-Glo assay 48 hours after drug addition. The *CDH1*$^{-/-}$ to MCF10A ratio is a measure of the reduced viability of the *CDH1*$^{-/-}$ cells in the presence of drug.

lethal drugs were selected for further characterization if they met two criteria: (i) modest toxicity to MCF10A cells (a decrease in viability of no more than 30%) and (ii) a minimum of 15% greater reduction in *CDH1*$^{-/-}$ viability compared with the MCF10A cells at one or more concentrations. Three-hundred sixteen compounds were selected for secondary analysis using an 11 point serial dilution from 10 μmol/L to 10 nmol/L. Twenty-one of 316 compounds in this secondary screen had EC_{50} values that were 10%–50% lower in the *CDH1*$^{-/-}$ cells compared with the MCF10A cells (Table 1). These included multiple histone deacetylase (HDAC) and PI3K inhibitors, crizotinib (an inhibitor of receptor tyrosine kinases c-MET, ALK, and ROS1), CGP 71683 hydrochloride (an inhibitor of the neuropeptide receptor NPY5R) and the guanine nucleotide exchange factor inhibitor Brefeldin A. The synthetic lethality of the majority of drug classes shown in Table 1 was supported by the siRNA primary screen data with one or more targets (or associated proteins) for each being included in List SL1 (Supplementary Table S4).

The E-cadherin synthetic lethal effects of crizotinib and several HDAC inhibitors were further characterized in time course and direct cell counting studies. Saracatinib, a c-SRC kinase inhibitor not included in the 11-point screen was also further examined because of a borderline effect in the original four-point screen. Crizotinib had little effect on the growth of MCF10A cells at 0.63, 1.25, and 2.50 μmol/L up to 48 hours after drug addition, as observed using the xCELLigence system. The same concentrations, however, reduced the growth of *CDH1*$^{-/-}$ cells to 86%, 76%, and 46% of mock (Fig. 4A). Nuclei counting at 48 hours confirmed the synthetic lethal effect, although an inhibitory effect was observed on the MCF10A cells at all three concentrations (Fig. 4B). The difference between the nuclei counting method and the IncuCyte and xCELLigence methods is primarily due to cell density differences at full confluency that can only be determined by direct nuclei counting.

Treatment with saracatinib caused greater growth inhibition in the *CDH1*$^{-/-}$ cells compared with the MCF10A cells at three different concentrations in two different assay systems, cell confluence (IncuCyte) and direct nuclei counting. In the IncuCyte system, a dose-dependent inhibition was observed in both isogenic cells with the *CDH1*$^{-/-}$ cells demonstrating greater susceptibility (Fig. 4C). At 0.63 μmol/L, saracatinib had negligible effect on the confluence of MCF10A cells but caused a 26% inhibition of *CDH1*$^{-/-}$ cells (relative to DMSO) after 48 hours. Similarly, differentials of 0.17 ($P = 0.06$), 0.30 ($P = 0.02$), and 0.15 ($P = 0.10$) were observed in normalized cell counts of the *CDH1*$^{-/-}$ cells compared with the MCF10A cells at saracatinib concentrations of 0.63, 1.25, and 2.5 μmol/L, respectively (Fig. 4D).

Entinostat selectively targets class I HDACs, in particular HDAC1–3 (26). The 0.63, 1.25, and 2.5 μmol/L entinostat had a negligible effect on cell proliferation of MCF10A as determined using the xCELLigence system. In contrast, *CDH1*$^{-/-}$ cells showed 18%, 67%, and 78% growth inhibition at these concentrations 48 hours after drug addition (Fig. 4E). Comparable results were obtained using the IncuCyte (Supplementary Fig. S3). Nuclei counting also showed a significant synthetic lethal effect across the three entinostat concentrations, although, as observed previously for crizotinib, reduced nuclei count was observed in both cell lines with increasing drug concentration using this more direct method. At concentrations of 0.63, 1.25, and 2.5 μmol/L, a cell viability differential of 0.13 ($P = 0.04$), 0.23 ($P = 0.004$), and 0.14 ($P = 0.02$) was observed between the *CDH1*$^{-/-}$ cells and the MCF10A cells (Fig. 4F).

Vorinostat (SAHA) is a pan-HDAC inhibitor, acting on both class I and class II HDACs (26). Assays using the IncuCyte system showed preferential inhibition of *CDH1*$^{-/-}$ cells over 48 hours of drug treatment at 0.63, 1.25, and 2.5 μmol/L, with little effect on the MCF10A cells (Fig. 4G). This effect was confirmed on the xCELLigence system (Supplementary Fig. S3). Similar to entinostat, direct nuclei counting showed a greater effect of vorinostat on the MCF10A cells than was observed using the real-time proliferation assay platforms. A significant cell viability differential was still observed between the *CDH1*$^{-/-}$ and MCF10A cells with cell

Published OnlineFirst March 16, 2015; DOI: 10.1158/1535-7163.MCT-14-1092

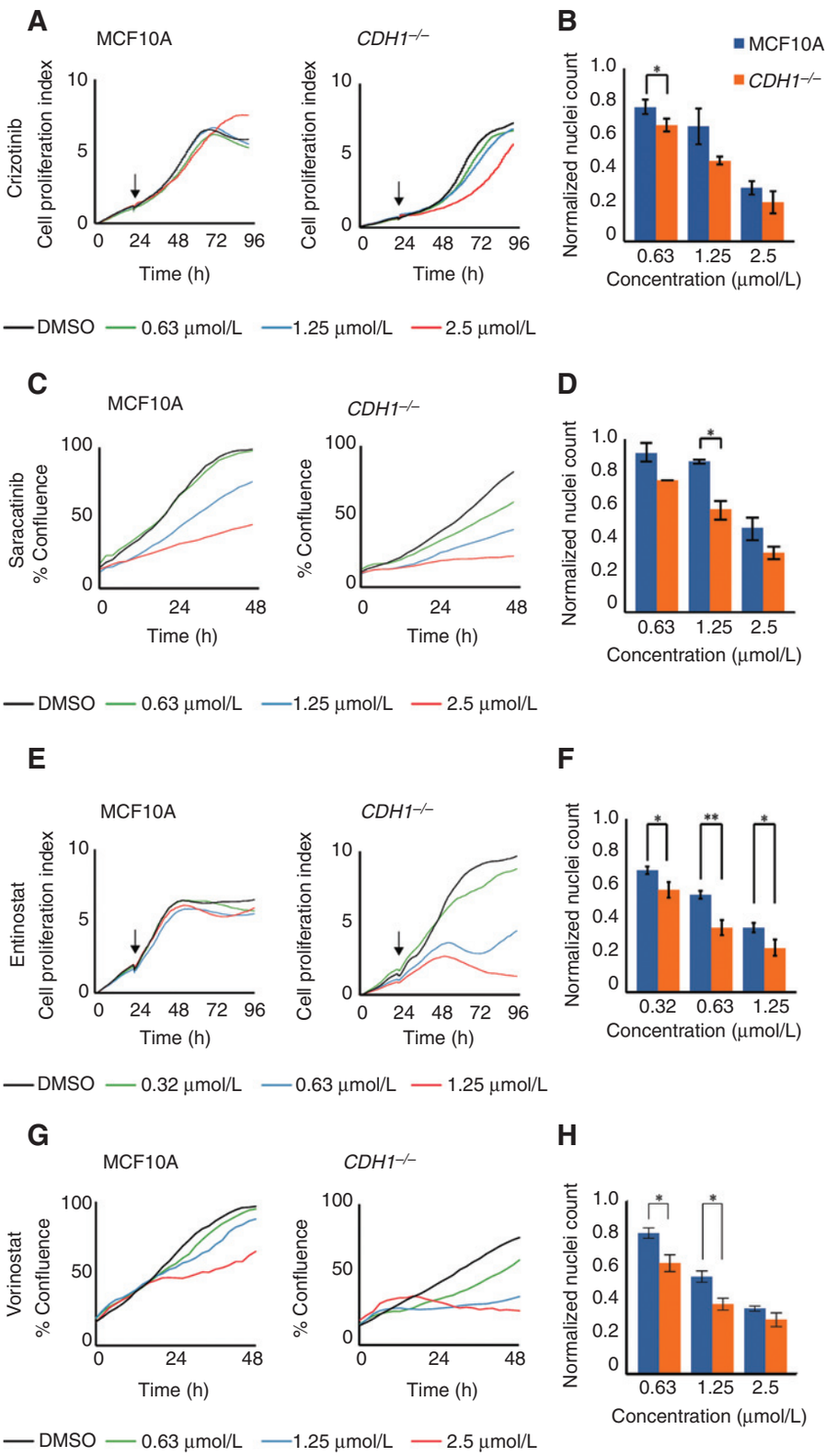

Figure 4.
Treatment with various known drugs causes *CDH1* synthetic lethality. A and E, representative xCELLigence assay of cells treated with crizotinib (A) and entinostat (E). Cells were seeded at 4,000 or 2,000 (crizotinib) cells per well and drug was added at 24 hours. Cells were grown for an additional 72 hours. C and G, representative IncuCyte assays of cells treated with saracatinib (C) and vorinostat (G). Cells were seeded at 4,000 cells per well and drug was added at 24 hours. Cells were then grown for an additional 48 hours. B, D, F and H, nuclei counts normalized to DMSO after treatment with crizotinib (B), saracatinib (D), entinostat (F), and vorinostat (H). Error bars show SE of at least two independent experiments. *, $P < 0.05$; **, $P < 0.01$ determined by the one-tailed, equal variance Student *t* test.

viability differentials of 0.21 ($P = 0.02$), 0.29 ($P = 0.01$), and 0.17 ($P = 0.10$) between *CDH1*$^{-/-}$ and MCF10A at concentrations of 0.63, 1.25, and 2.5 μmol/L (Fig. 4H). The HDAC inhibitors mocetinostat and pracinostat showed comparable synthetic lethal effects when assayed at 0.63, 1.25, and 2.5 μmol/L on the xCELLigence system (Supplementary Fig. S4A and S4B). The class

Published OnlineFirst March 16, 2015; DOI: 10.1158/1535-7163.MCT-14-1092

I/II HDAC inhibitor valproic acid also showed a minor synthetic lethal effect when assayed by direct nuclei counting (Supplementary Fig. S4C).

Previous reports of synergy between HDAC inhibitors and taxol (27–30) prompted us to test combinations of taxol and each of vorinostat and entinostat in our isogenic cell line pair. CompuSyn (ComboSyn Inc) was used to calculate EC_{50} concentrations, and to determine the Combination Index. In contrast to other studies, we found no evidence for synergy between taxol and these HDAC inhibitors (Supplementary Fig. S2).

Discussion

Synthetic lethality provides a potential method to target cancers carrying inactivating mutations in tumor suppressor genes such as the E-cadherin gene, *CDH1*. To provide an initial survey of E-cadherin's synthetic lethal interactions, we conducted a genome-wide functional screen of nonmalignant, isogenic MCF10A cells with and without E-cadherin expression. Thirteen percent of the 18,120 genes in the siRNA screen met our threshold for synthetic lethality of at least 15% more death in the $CDH1^{-/-}$ cells than the wild-type MCF10A cells. Although this threshold is low stringency and subsequently not highly specific, it is clear that E-cadherin deficiency creates large numbers of vulnerabilities in nonmalignant cells which are exposed by genetic knockdown of additional genes.

Gene ontology analysis identified a striking enrichment for GPCR signaling proteins among the synthetic lethal candidates. Notably, this enrichment was greater for hits that showed minimal impact on the viability of the E-cadherin–expressing MCF10A cells, suggesting that drug targeting of GPCR signaling in *CDH1*-mutant tumors may be a means to obtain clinical gain while minimizing collateral damage to normal tissues. The nature of the synthetic lethal relationship between E-cadherin and GPCR signaling is not yet known, although the functional diversity of the candidate synthetic lethal GPCR signaling proteins would suggest that the interaction involves a common downstream mechanism such as interplay with the actin and microtubule cytoskeletons (31–33). The importance of cytoskeletal functions to the E-cadherin synthetic lethal phenotype is supported by the abundance of cytoskeletal genes associated with synthetic lethality in our primary siRNA screen. These genes were involved in all aspects of cytoskeletal function, including the nucleation, organization, and function of microtubules mitotic spindle organization and control, linkages between the cytoskeleton and nucleoskeleton, polarity, actin filament organization, vesicle transport, focal adhesion kinase signaling, and Rho-mediated motility (8, 34–36). The increased vulnerability of E-cadherin–deficient MCF10A cells to knockdown of so many diverse but inter-related functions is consistent with the widespread disorganization of cytoskeletal networks observed in the $CDH1^{-/-}$ cells (7). Notably, after *CDH1* and *TP53*, *RHOA* is the most commonly mutated gene in DGC (37–39), emphasizing the importance of dysregulated cytoskeletal function to development of the diffuse phenotype.

The increased vulnerability of E-cadherin–deficient MCF10A cells to RNAi knockdown of cytoskeletal and GPCR signaling genes was supported by the increased sensitivity of these cells to antagonists of multiple protein families associated with GPCR signaling and cytoskeletal function, including HDACs (40, 41), JAK (42), aurora kinases (43), c-SRC tyrosine kinase (44), G-protein subunits and PI3K (45). The enrichment for GPCR signaling genes among our synthetic lethal candidates does not, however, exclude the possibility that other signaling functions, such as the cytokine responses of JAK2, may also be associated with synthetic lethality. EC_{50} differences between MCF10A and $CDH1^{-/-}$ cells for these known drugs were on average only approximately 25% less in the $CDH1^{-/-}$ cells. This small differential is to be expected as neither MCF10A or $CDH1^{-/-}$ cells are tumorigenic and therefore these lines cannot be distinguished by the presence/absence of addiction to the targeted pathways. Synthetic lethal drugs which are significantly more potent in E-cadherin–deficient cells will be more readily identified using fit-for-purpose, high-throughput compound screens across the MCF10A and other *CDH1* isogenic cell line pairs. Differences between the E-cadherin–expressing and E-cadherin–deficient cells may also be more pronounced in phenotypes other than cell viability, such as invasive capability.

This research demonstrates for the first time that loss of the tumor suppressor protein E-cadherin creates druggable vulnerabilities in cells. It remains to be determined whether any of the observed drug sensitivities in $CDH1^{-/-}$ cells will be robust to the genetic dysregulation of advanced tumors, and therefore able to provide additional clinical benefit in the treatment of sporadic *CDH1*-mutant tumors. Instead, the observed sensitivities may have more near term application to HDGC chemoprevention. The natural history of cancer development in *CDH1* germline mutation carriers involves the development of multifocal lobular carcinoma *in situ* (46, 47) and tens to hundreds of gastric stage T1a signet ring cell carcinomas before the onset of advanced disease (11, 48, 49). The high multiplicity of these early stage foci argues against additional genetic hits being required for their initiation. These early breast and gastric cancers are therefore relatively genetically homogenous and distinguished from normal tissue predominantly by the cellular changes associated with deficiency of E-cadherin. As a consequence, the E-cadherin synthetic lethal interactions identified in the nonmalignant breast MCF10A cells provide strong leads for drugs that may eliminate early-stage disease in germline *CDH1* mutation carriers, potentially providing a new clinical management option for HDGC families.

Disclosure of Potential Conflicts of Interest

No potential conflicts of interest were disclosed.

Authors' Contributions

Conception and design: A. Chen, K.J. Simpson, P. Guilford
Development of methodology: B.J. Telford, A. Chen, H. Beetham, J. Frick, T.P. Brew, A. Single, T. Godwin, K.J. Simpson, P. Guilford
Acquisition of data (provided animals, acquired and managed patients, provided facilities, etc.): B.J. Telford, A. Chen, J. Frick, T.P. Brew, A. Single, T. Godwin, K.J. Simpson, P. Guilford
Analysis and interpretation of data (e.g., statistical analysis, biostatistics, computational analysis): B.J. Telford, A. Chen, J. Frick, T.P. Brew, C.M. Gould, A. Single, K.J. Simpson, P. Guilford
Writing, review, and/or revision of the manuscript: B.J. Telford, A. Chen, H. Beetham, T.P. Brew, A. Single, K.J. Simpson, P. Guilford
Administrative, technical, or material support (i.e., reporting or organizing data, constructing databases): B.J. Telford, A. Chen, H. Beetham, C.M. Gould, P. Guilford
Study supervision: A. Chen, K.J. Simpson, P. Guilford

Acknowledgments

VCFG technical expertise was provided by Daniel Thomas and Yanny Handoko. Lentiviral expertise and training was provided by Dr. Stephanie Hughes and Hollie Wicky. Compound screening was performed at the Walter Eliza Hall Institute under the supervision of Dr. Kurt Lackovic.

Grant Support

This work was supported by the New Zealand Health Research Council (grant number 11/513 to P. Guilford) and the University of Otago (PhD Fellowships to B. Telford, H. Beetham, and A. Single). Additional funding support was received from No Stomach for Cancer Inc, the Degregario Family Foundation and the New Zealand Breast Cancer Research Partnership. The Victorian Centre for Functional Genomics (to K. Simpson) is funded by the Australian Cancer Research Foundation (ACRF), the Victorian Department of Industry, Innovation and Regional Development (DIIRD), the Australian Phenomics Network (APN) supported by funding from the Australian Government's Education Investment Fund through the Super Science Initiative, the Australasian Genomics Technologies Association (AMATA), the Brockhoff Foundation, and the Peter MacCallum Cancer Centre Foundation.

The costs of publication of this article were defrayed in part by the payment of page charges. This article must therefore be hereby marked *advertisement* in accordance with 18 U.S.C. Section 1734 solely to indicate this fact.

Received December 26, 2014; revised February 16, 2015; accepted March 6, 2015; published OnlineFirst March 16, 2015.

References

1. Berx G, van Roy F. Involvement of members of the cadherin superfamily in cancer. Cold Spring Harb Perspect Biol 2009;1:a003129.
2. Mohamet L, Hawkins K, Ward CM. Loss of function of e-cadherin in embryonic stem cells and the relevance to models of tumorigenesis. J Oncol 2011;2011:352616.
3. Jeanes A, Gottardi CJ, Yap AS. Cadherins and cancer: how does cadherin dysfunction promote tumor progression? Oncogene 2008;27:6920–9.
4. Guilford P, Hopkins J, Harraway J, McLeod M, McLeod N, Harawira P, et al. E-cadherin germline mutations in familial gastric cancer. Nature 1998; 392:402–5.
5. Corso G, Carvalho J, Marrelli D, Vindigni C, Carvalho B, Seruca R, et al. Somatic mutations and deletions of the E-cadherin gene predict poor survival of patients with gastric cancer. J Clin Oncol 2013;31:868–75.
6. Vlug E, Ercan C, van der Wall E, van Diest PJ, Derksen PW. Lobular breast cancer: pathology, biology, and options for clinical intervention. Arch Immunol Ther Exp 2013;62:7–21.
7. Chen A, Beetham H, Black MA, Priya R, Telford BJ, Guest J, et al. E-cadherin loss alters cytoskeletal organization and adhesion in non-malignant breast cells but is insufficient to induce an epithelial-mesenchymal transition. BMC Cancer 2014;14:552.
8. Brieher WM, Yap AS. Cadherin junctions and their cytoskeleton(s). Curr Opin Cell Biol 2013;25:39–46.
9. den Elzen N, Buttery CV, Maddugoda MP, Ren G, Yap AS. Cadherin adhesion receptors orient the mitotic spindle during symmetric cell division in mammalian epithelia. Mol Biol Cell 2009;20:3740–50.
10. Zou D, Yoon HS, Perez D, Weeks RJ, Guilford P, Humar B. Epigenetic silencing in non-neoplastic epithelia identifies E-cadherin (CDH1) as a target for chemoprevention of lobular neoplasia. J Pathol 2009;218: 265–72.
11. Humar B, Blair V, Charlton A, More H, Martin I, Guilford P. E-cadherin deficiency initiates gastric signet-ring cell carcinoma in mice and man. Cancer Res 2009;69:2050–6.
12. Humar B, Guilford P. Hereditary diffuse gastric cancer and lost cell polarity: a short path to cancer. Future Oncol (London, England) 2008;4:229–39.
13. Thiery JP, Acloque H, Huang RY, Nieto MA. Epithelial-mesenchymal transitions in development and disease. Cell 2009;139:871–90.
14. Fong PC, Yap TA, Boss DS, Carden CP, Mergui-Roelvink M, Gourley C, et al. Poly(ADP)-ribose polymerase inhibition: frequent durable responses in BRCA carrier ovarian cancer correlating with platinum-free interval. J Clin Oncol 2010;28:2512–9.
15. Gelmon KA, Tischkowitz M, Mackay H, Swenerton K, Robidoux A, Tonkin K, et al. Olaparib in patients with recurrent high-grade serous or poorly differentiated ovarian carcinoma or triple-negative breast cancer: a phase 2, multicentre, open-label, non-randomised study. Lancet Oncol 2011; 12:852–61.
16. Kamentsky L, Jones TR, Fraser A, Bray MA, Logan DJ, Madden KL, et al. Improved structure, function and compatibility for CellProfiler: modular high-throughput image analysis software. Bioinformatics 2011;27:1179–80.
17. Pfaffl MW. A new mathematical model for relative quantification in real-time RT-PCR. Nucleic Acids Res 2001;29:2002–7.
18. Chou TC, Talalay P. Quantitative analysis of dose-effect relationships: the combined effects of multiple drugs or enzyme inhibitors. Adv Enzyme Regul 1984;22:27–55.
19. Petrocca F, Altschuler G, Tan SM, Mendillo ML, Yan H, Jerry DJ, et al. A genome-wide siRNA screen identifies proteasome addiction as a vulnerability of basal-like triple-negative breast cancer cells. Cancer Cell 2013;24:182–96.
20. Lee AS, Burdeinick-Kerr R, Whelan SP. A genome-wide small interfering RNA screen identifies host factors required for vesicular stomatitis virus infection. J Virol 2014;88:8355–60.
21. Huang da W, Sherman BT, Lempicki RA. Systematic and integrative analysis of large gene lists using DAVID bioinformatics resources. Nat Protoc 2009;4:44–57.
22. Garland P, Quraishe S, French P, O'Connor V. Expression of the MAST family of serine/threonine kinases. Brain Res 2008;1195:12–9.
23. Villarroel-Campos D, Gonzalez-Billault C. The MAP1B case: an old MAP that is new again. Dev Neurobiol 2014;74:953–71.
24. Akhmanova A, Steinmetz MO. Tracking the ends: a dynamic protein network controls the fate of microtubule tips. Nat Rev Mol Cell Biol 2008;9:309–22.
25. Clark MJ, Traynor JR. Assays for G-protein-coupled receptor signaling using RGS-insensitive Galpha subunits. Methods Enzymol 2004;389:155–69.
26. Dickinson M, Johnstone RW, Prince HM. Histone deacetylase inhibitors: potential targets responsible for their anti-cancer effect. Invest New Drugs 2010;28 Suppl 1:S3–20.
27. Shi YK, Li ZH, Han XQ, Yi JH, Wang ZH, Hou JL, et al. The histone deacetylase inhibitor suberoylanilide hydroxamic acid induces growth inhibition and enhances taxol-induced cell death in breast cancer. Cancer Chemother Pharmacol 2010;66:1131–40.
28. Dietrich CS III, Greenberg VL, DeSimone CP, Modesitt SC, van Nagell JR, Craven R, et al. Suberoylanilide hydroxamic acid (SAHA) potentiates paclitaxel-induced apoptosis in ovarian cancer cell lines. Gynecol Oncol 2010;116:126–30.
29. Owonikoko TK, Ramalingam SS, Kanterewicz B, Balius TE, Belani CP, Hershberger PA. Vorinostat increases carboplatin and paclitaxel activity in non-small-cell lung cancer cells. Int J Cancer 2010;126:743–55.
30. Dowdy SC, Jiang S, Zhou XC, Hou X, Jin F, Podratz KC, et al. Histone deacetylase inhibitors and paclitaxel cause synergistic effects on apoptosis and microtubule stabilization in papillary serous endometrial cancer cells. Mol Cancer Ther 2006;5:2767–76.
31. Ganguly S, Saxena R, Chattopadhyay A. Reorganization of the actin cytoskeleton upon G-protein coupled receptor signaling. Biochim Biophys Acta 2011;1808:1921–9.
32. Schappi JM, Krbanjevic A, Rasenick MM. Tubulin, actin and heterotrimeric G proteins: coordination of signaling and structure. Biochim Biophys Acta 2014;1838:674–81.
33. Saengsawang W, Rasenick MM. Heterotrimeric G proteins and microtubules. Methods Cell Biol 2013;115:173–89.
34. Kollman JM, Merdes A, Mourey L, Agard DA. Microtubule nucleation by gamma-tubulin complexes. Nat Rev Mol Cell Biol 2011;12:709–21.
35. Sulzmaier FJ, Jean C, Schlaepfer DD. FAK in cancer: mechanistic findings and clinical applications. Nat Rev 2014;14:598–610.
36. Hall A. The cytoskeleton and cancer. Cancer Metastasis Rev 2009;28:5–14.
37. Kakiuchi M, Nishizawa T, Ueda H, Gotoh K, Tanaka A, Hayashi A, et al. Recurrent gain-of-function mutations of RHOA in diffuse-type gastric carcinoma. Nat Genet 2014;46:583–7.
38. Cancer Genome Atlas Research N. Comprehensive molecular characterization of gastric adenocarcinoma. Nature 2014;513:202–9.
39. Wang K, Yuen ST, Xu J, Lee SP, Yan HH, Shi ST, et al. Whole-genome sequencing and comprehensive molecular profiling identify new driver mutations in gastric cancer. Nat Genet 2014;46:573–82.

40. Spiegelberg BD. G protein coupled-receptor signaling and reversible lysine acetylation. J Recept Signal Transduct Res 2013;33:261–6.
41. Schemies J, Sippl W, Jung M. Histone deacetylase inhibitors that target tubulin. Cancer Lett 2009;280:222–32.
42. Pelletier S, Duhamel F, Coulombe P, Popoff MR, Meloche S. Rho family GTPases are required for activation of Jak/STAT signaling by G protein-coupled receptors. Mol Cell Biol 2003;23:1316–33.
43. Hochegger H, Hegarat N, Pereira-Leal JB. Aurora at the pole and equator: overlapping functions of Aurora kinases in the mitotic spindle. Open Biol 2013;3:120185.
44. Luttrell LM, Hawes BE, van Biesen T, Luttrell DK, Lansing TJ, Lefkowitz RJ. Role of c-Src tyrosine kinase in G protein-coupled receptor- and Gbeta-gamma subunit-mediated activation of mitogen-activated protein kinases. J Biol Chem 1996;271:19443–50.
45. Fritsch R, de Krijger I, Fritsch K, George R, Reason B, Kumar MS, et al. RAS and RHO families of GTPases directly regulate distinct phosphoinositide 3-kinase isoforms. Cell 2013;153:1050–63.
46. Blair VR. Hereditary diffuse gastric cancer: Of mice and man. Auckland, New Zealand: PhD thesis, University of Auckland; 2008.
47. Petridis C, Shinomiya I, Kohut K, Gorman P, Caneppele M, Shah V, et al. Germline CDH1 mutations in bilateral lobular carcinoma in situ. Br J Cancer 2014;110:1053–7.
48. Charlton A, Blair V, Shaw D, Parry S, Guilford P, Martin IG. Hereditary diffuse gastric cancer: predominance of multiple foci of signet ring cell carcinoma in distal stomach and transitional zone. Gut 2004;53:814–20.
49. Fitzgerald RC, Hardwick R, Huntsman D, Carneiro F, Guilford P, Blair V, et al. Hereditary diffuse gastric cancer: updated consensus guidelines for clinical management and directions for future research. J Med Genet 2010;47:436–44.

Published OnlineFirst March 16, 2015; DOI: 10.1158/1535-7163.MCT-14-1092

Molecular Cancer Therapeutics

Synthetic Lethal Screens Identify Vulnerabilities in GPCR Signaling and Cytoskeletal Organization in E-Cadherin –Deficient Cells

Bryony J. Telford, Augustine Chen, Henry Beetham, et al.

Mol Cancer Ther 2015;14:1213-1223. Published OnlineFirst March 16, 2015.